Angle-Resolved Photoemission Spectroscopy Study of Adsorption Process and Electronic Structure of Silver on ZnO($10\bar{1}0$)

K. Ozawa,*,† T. Sato,† M. Kato,† K. Edamoto,‡ and Y. Aiura§

Department of Chemistry and Materials Science, Tokyo Institute of Technology, Ookayama, Meguro-ku, Tokyo 152-0033, Japan, Department of Chemistry, Rikkyo University, Nishi-Ikebukuro, Toshima-ku, Tokyo 171-8501, Japan, and National Institute of Advanced Industrial Science and Technology, Tsukuba, Ibaraki 305-8568, Japan

Received: April 15, 2005; In Final Form: June 10, 2005

The adsorption process and valence band structure of Ag on ZnO($10\bar{1}0$) have been investigated by angle-resolved photoelectron spectroscopy utilizing synchrotron radiation. The coverage-dependent measurements of the Ag 4d band structure reveal that the Ag bands with a dispersing feature are formed even at low coverages and that the basic structure of the bands is essentially the same throughout the submonolayer region. These results indicate that the Ag atoms aggregate to form islands with an atomically ordered structure from the low coverages. Upon annealing the Ag-covered surface at 900 K, the Ag 4d band undergoes only a minor change, suggesting that the ordered structure within the Ag islands is persistent against mild annealing. From the dispersive feature of the Ag 4d states, we propose that the atomic structure has locally rectangular symmetry with a good lattice matching with the ZnO($10\bar{1}0$) surface.

Introduction

Adsorption of metals on oxide surfaces and the formation of metal/oxide complex systems are technically and scientifically important processes because the metal/oxide system plays a crucial role in many applications such as microelectronic devices and chemical sensors. Moreover, metals supported on the oxide surfaces often exhibit peculiar chemical reactivity that the bulk metals do not possess, and thus many of these systems are utilized as heterogeneous catalysts. A well-known example is Au, which is classified as a chemically inert material in the bulk form but acts as a good catalyst in a variety of chemical reactions in the form of small clusters.[1] Recent studies by Goodman and co-workers[2,3] have indicated a clear relevance between high chemical reactivity and the morphology of the Au clusters, that is, the Au adatoms on TiO_2(110) show maximum reactivity for CO oxidation when they form bilayer clusters, whose electronic structure is on the verge of the nonmetal-to-metal transition. Thus, the morphology and the electronic properties of metal clusters on the oxide surfaces are of great interest.

ZnO is one of the frequently available oxide supports; for example, the Cu/ZnO-based catalysts have been used for synthesis of methanol[4,5] and higher alcohols,[6,7] water gas shift reaction,[5] steam reforming of methanol,[8] and so forth. Similar catalytic activity is also found for Pd/ZnO,[9] Pt/ZnO,[10] Au/ZnO,[11] and Ag/ZnO[12,13] systems. Therefore, growth of these metals on the low-index surfaces of single-crystal ZnO has been the subject of extensive studies. Campbell and co-workers have investigated the Cu growth mode on the polar ZnO(0001)−Zn and (0001)−O surfaces using low energy ion scattering spectroscopy (LEIS), X-ray photoelectron spectroscopy (XPS), and low energy electron diffraction (LEED)[14−16] and found that the Cu overlayer grows as two-dimensional (2D) islands at low coverages, whereas three-dimensional (3D) growth sets in at the "critical" coverages, which are below the monolayer coverage. The scanning tunneling microscopy (STM) study[17] has confirmed the same growth mode of Cu on ZnO(0001)−Zn, but with much smaller critical coverage than that derived from the studies using the nonimaging techniques. Cu on ZnO($10\bar{1}0$) seems to skip the formation of the 2D islands, and 3D island growth proceeds from the very low coverages.[18] In contrast, a 2D flat layer formation up to the completion of the first monolayer has been proposed from the Auger electron spectroscopy (AES) study for Pd on both polar ZnO surfaces.[19] The layer formation up to the monolayer coverage has also been proposed for Pt on the polar ZnO surfaces by several authors,[20−22] whereas the 2D−3D transition mechanism of Pt on ZnO($000\bar{1}$)−O has been suggested by recent LEIS and XPS studies.[23] Regarding adsorption of Ag, which is the subject of the present study, growth of Ag on the polycrystalline ZnO surface has been investigated by XPS and found to proceed via the 2D−3D transition.[24] No report has been available yet for the growth mode of Ag on the single-crystal ZnO surfaces.

ZnO($10\bar{1}0$) has a unique surface structure, which is characterized by the Zn−O dimer rows running along the [$\bar{1}2\bar{1}0$] direction. Diffusion of adatoms on the ($10\bar{1}0$) surface is, therefore, constrained along the dimer rows[18] so that a unique adsorption structure is expected. In fact, the 1D structure of adsorbed K along the dimer rows has been suggested from the XPS and LEED measurements.[25] However, in contrast to the case of the polar ZnO surfaces, little is understood about the behavior of metals on the nonpolar ZnO($10\bar{1}0$) surface.

The morphology of metal adlayers on the oxide surfaces defines the electronic structure of the metal overlayers and hence influences their chemical nature. However, in all of the above-mentioned studies for the metal/ZnO systems, details on the electronic structure, especially on the valence band structure,

* To whom correspondence should be addressed. Fax: +81 3 5734 2655. E-mail: kozawa@chem.titech.ac.jp.
† Tokyo Institute of Technology.
‡ Rikkyo University.
§ National Institute of Advanced Industrial Science and Technology.

10.1021/jp051975e CCC: $30.25
Published on Web 07/08/2005

of the deposited metal films have not been clarified. Thus, it is desired to shed light on the electronic structure of deposited metal overlayers. In the present study, we have investigated the valence band structure of the vapor-deposited Ag overlayer on ZnO(10$\bar{1}$0) using angle-resolved photoelectron spectroscopy (ARPES). The coverage-dependent change and the annealing effect of the Ag valence band structure have been examined. From the evolution of the Ag 4d bands as a function of the Ag coverage, it is indicated that adsorption of Ag proceeds via the formation of islands with an atomically ordered structure. The growth mode with the 2D−3D transition is also suggested.

Experimental Section

The experiments were performed at the beam lines (BL) 1C and 11C of the Photon Factory, High Energy Accelerator Research Organization (KEK), utilizing the linearly polarized synchrotron radiation. The measurements at BL 11C were carried out in a ultrahigh vacuum (UHV) chamber with a base pressure of 2×10^{-10} Torr. The UHV chamber was equipped with a hemispherical electron energy analyzer (VSW HA54) with a microchannel-plate electron multiplier (MCP) detector for the ARPES measurements, a single-pass cylindrical mirror analyzer for the AES measurements, LEED optics, and a quadrupole mass spectrometer. The ARPES spectra were taken at a photon energy, $h\nu$, of 20 eV with a total experimental resolution of 210 meV. For the ARPES measurements at BL 1C, the different UHV apparatus (the base pressure of 5×10^{-10} Torr), equipped with a hemispherical electron energy analyzer (VG ARUPS10), was used. In the experiment at this beam line, the ZnO sample was mounted on the goniometer (R-Dec, *i* Gonio LT),[26] which enables the independent polar, azimuth, and tilt rotations of the sample so that the polarization-dependent measurements utilizing the *s*-polarized light were possible. The spectra were measured at $h\nu = 40$ eV with the total experimental resolution of 100 meV. All of the measurements at BL 1C and 11C were carried out at room temperature.

Several ZnO single crystals with the (10$\bar{1}$0) orientation ($7 \times 5 \times 0.5$ mm^3; Yamanaka Semiconductor Co.) were used throughout the experiments. A well-established procedure was taken for cleaning the sample surface in the UHV chamber.[25] Briefly, cycles of Ar^+ sputtering (1.6 kV, 2−3 μA) and annealing at 1050 K in UHV were followed by annealing at 700 K in O_2 atmosphere and 600 K in UHV. The electron bombardment from the rear of the sample, which was mounted on the Ta or Mo sample holder, was employed for annealing. The sample temperature was monitored by a chromel−almel thermocouple attached to the sample holder. The cleanliness of the surface was checked by measuring the AES and ARPES spectra, which showed no peaks associated with contaminants such as carbon and hydroxide. The clean surface exhibited a LEED pattern with sharp (1×1) spots. The work function, determined from the spectral width from the Fermi level to the secondary electron cutoff, was 4.5 eV, in good agreement with the literature values.[27−29]

Ag was vapor-deposited onto the surface at room temperature from the evaporation source (Omicron EFM3). Ag was evaporated from a high-purity Ag rod (99.995%) of 2 mm diameter by electron bombardment, and the deposition rate was controlled by monitoring a flux current of Ag cations at the exit of the evaporation source. The pressure of the chamber during the deposition was kept below 8×10^{-10} Torr to avoid a possible contamination of the deposited Ag film.

In the ARPES spectra presented below, the binding energy is referenced to zero at the Fermi energy (E_F), which was determined from the spectra of the sample holders. The incidence angle of the light beam, θ_i, and the detection angle of the photoelectrons, θ_d, are given relative to the surface normal direction.

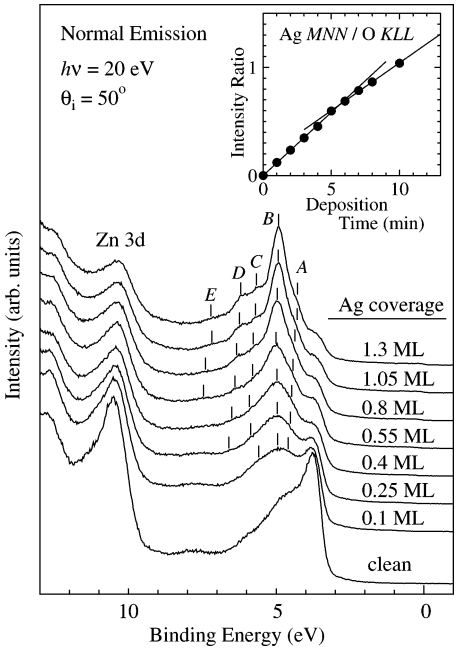

Figure 1. Normal emission spectra of Ag/ZnO(10$\bar{1}$0) as a function of the Ag coverage. The positions of the Ag 4d peaks are determined from the second derivatives of the measured spectra and are indicated by tick marks. The inset shows the Ag deposition-time dependence of the intensity ratio between the Ag *MNN* and O *KLL* Auger peaks. A kink structure is seen at 5.5 min.

Results

Ag Adsorption at Room Temperature. Figure 1 shows the change in the normal emission spectrum of the ZnO(10$\bar{1}$0) surface as a function of the Ag coverage. The photon energy used was 20 eV, and the incidence angle of the light, θ_i, was 50 ° from the surface normal. The spectrum of the clean surface is characterized by a sharp peak at 3.7 eV and several weaker peaks between 4 and 8 eV, which are associated with the emission from the O 2p dangling-bond state and O 2p-Zn 3d/4sp hybrid states, respectively. The emission peak at 10−11 eV is attributed to the Zn 3d state. The electronic structure of the clean ZnO(10$\bar{1}$0) surface has been discussed in detail in our previous papers.[30,31] As the surface is being covered with Ag, the Ag 4d peaks grow at 4−8 eV, whereas the emission from the substrate surface is gradually suppressed. The positions of the Ag 4d states are determined by taking second derivatives of the observed spectra and are indicated by tick marks in Figure 1. Five peaks, labeled *A*−*E*, are identified at high Ag coverages.

In the inset of Figure 1, we show the change in the Auger peak-to-peak intensity ratio of Ag *MNN*/O *KLL* as a function of the deposition time. The intensity ratio increases linearly with deposition time, whereas the slope diminishes at deposition times larger than 5.5 min. The same behavior is also observed for the Ag *MNN*/Zn *LMM* intensity ratio. In this paper, we define the kink point as one Ag monolayer (ML), and the Ag coverage Θ_{Ag} at each deposition time is estimated from the Ag *MNN*/O *KLL* intensity ratio relative to that at the kink point.

To determine the atomic density of the Ag overlayer at 1 ML, we have further carried out the following analysis: The deposition time dependence of the Ag *MNN*/O *KLL* ratio for the Ag/ZnO(10$\bar{1}$0) system gives a characteristic discontinuity

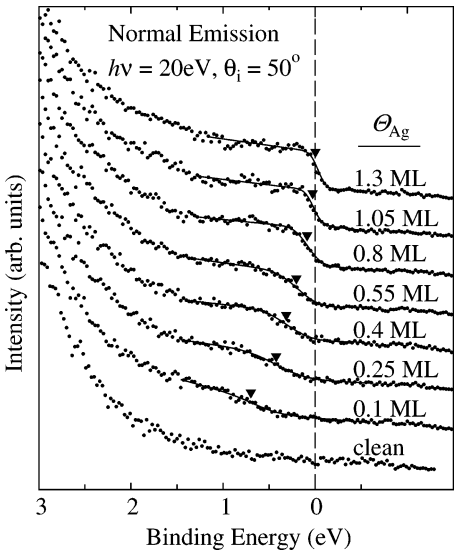

Figure 2. Enlarged spectra around the gap region of ZnO. Growth of the Ag 5sp DOS is observed. The onset structure of the DOS is reproduced by the Gaussian-convoluted Fermi distribution function as shown by solid lines. The midpoint of the onset energy, indicated by triangles, locates at 0.7 eV at 0.1 ML and moves to E_F at ~1 ML.

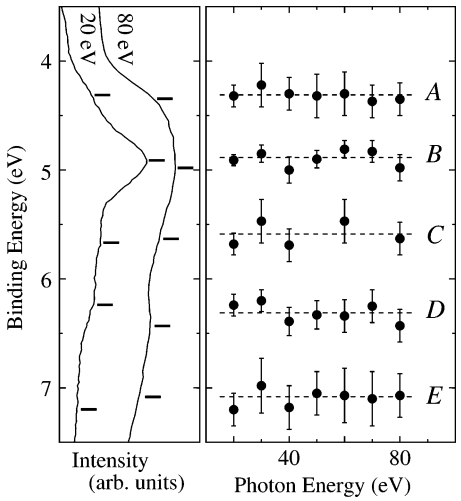

Figure 3. (left) Normal emission spectra for the 1.3-ML Ag-covered ZnO(10$\bar{1}$0) surface taken at $h\nu = 20$ and 80 eV. The position of the Ag 4d states is indicated by tick marks. (right) The plot of the binding energy of the Ag 4d states in the normal emission spectra as a function of $h\nu$.

as shown in the inset of Figure 1. Similarly, the plot of the intensity ratio of Ag *MNN*/Cu *MVV* for the Ag/Cu(001) system, obtained by the different experiment but with the same experimental condition including the Ag deposition rate, shows a kink structure (result not shown). For both Ag adsorption systems, it is found that the Ag *MNN* peak intensity at the kink points is the same within the experimental error. This suggests that the density of the Ag adatoms at 1 ML on ZnO(10$\bar{1}$0) should be nearly equal to that at the kink point on Cu(001). It is known that the kink in the Ag *MNN*/Cu *MVV* plot for the Ag/Cu(001) system corresponds to the completion of the Ag monolayer, whose atomic density is the same as the packing density of Ag(111), that is, 1.381×10^{15} atoms/cm^2.[32,33] Thus, the Ag density at 1 ML on ZnO(10$\bar{1}$0) is estimated to be approximately 1.4×10^{15} atoms/cm^2.

It should be noted that the observation of the kink in the Ag *MNN*/O *KLL* plot does not mean the formation of the 2D Ag overlayer up to the completion of the monolayer. As will be discussed below, although the 2D Ag islands are formed at low coverages, 3D growth seems to start well below 1 ML. Thus, the origin of the kink structure is not known at present.

The LEED measurements show that the Ag-covered surface gives blurred (1×1) spots on an intense background at any Θ_{Ag} below 1.3 ML. This indicates that the adsorbed Ag atoms do not form any long-range ordered superstructures on ZnO(10$\bar{1}$0) at room temperature.

In addition to the strong Ag 4d emission peaks from the Ag-covered ZnO(10$\bar{1}$0) surface, we have also observed growth of the emission from the Ag 5sp states in the band gap region of ZnO with increasing Θ_{Ag}. Figure 2 shows the enlarged spectra around E_F of Figure 1. Two Θ_{Ag}-dependent changes are noticeable; one is that the emission intensity of the Ag 5sp states is gradually enlarged so that the step structure becomes obvious, and the other is that the onset of the step, which is located well below E_F at 0.1 ML, moves toward E_F with increasing Θ_{Ag}. These Θ_{Ag} dependences should represent the changes of the total density of states (DOS) of the Ag 5sp bands, because the off-normal emission spectra also exhibit the step structure similar to that shown in Figure 2. The triangles in Figure 2 indicate the precise positions of the onset of the Ag 5sp DOS, determined by fitting the observed spectra using a Gaussian-convoluted Fermi distribution function and a polynomial background curve. The onset of the Ag 5sp DOS locates at 0.7 eV at 0.1 ML, and it coincides with E_F at $\Theta_{Ag} \geq 1$ ML. Such a change in the onset energy is characteristic for the metal adsorption systems on oxide surfaces, where adsorbed metal atoms aggregate to form clusters and these clusters grow in size with increasing coverages.[34−36] Thus, the spectral change in Figure 2 suggests that the Ag adatoms should aggregate to form islands on ZnO(10$\bar{1}$0).

Figure 3 shows the normal emission spectra for the 1.3-ML Ag-covered ZnO(10$\bar{1}$0) surface taken at $h\nu = 20$ and 80 eV (left panel) and the $h\nu$-dependence of the binding energy of the Ag 4d states (*A*-*F*) observed in the normal emission spectra measured at $h\nu = 20-80$ eV (right panel). It is seen that each Ag 4d state appears at nearly the same binding energy irrespective of $h\nu$. This implies that the Ag 4d states do not depend on the surface perpendicular component of the wave vector $k_\perp$. However, these states show a clear dispersion as a function of the surface parallel component of the wave vector $k_{||}$, as will be discussed below. Thus, the Ag 4d states have 2D character. The lack of the $k_\perp$-dependent dispersion of the Ag 4d states implies that, although the Ag adatoms form the islands on ZnO(10$\bar{1}$0), they should be monolayer-thick 2D islands and/or thin 3D islands with a few atomic-layer thickness.

To see the electronic structure of the Ag islands in more detail, the $k_{||}$ dependence of the Ag 4d states is examined. Figure 4a shows the off-normal emission spectra of the 0.65-ML Ag-covered ZnO(10$\bar{1}$0) surface. The detection plane of the photoelectrons was set parallel to the [0001] direction of the substrate surface, and thus the states along the $\overline{\Gamma X'}$ axis of the surface Brillouin zone (SBZ) of the substrate surface were probed. In the normal emission spectrum, the Ag 4d peaks (*A*−*E*) are observed at 4.5, 5.1, 5.8, 6.4, and 7.2 eV. Increase in θ_d leads to the shift of some of the Ag 4d peaks, implying that the binding energy of the Ag 4d states depends on $k_{||}$. In Figure 4b, we plot the peak positions against $k_{||}$ along the $\overline{\Gamma X'}$ axis by open circles on a grayscale map, which is obtained by plotting the spectral weight of the second derivatives of the off-normal emission spectra. $k_{||}$ is calculated from θ_d and the

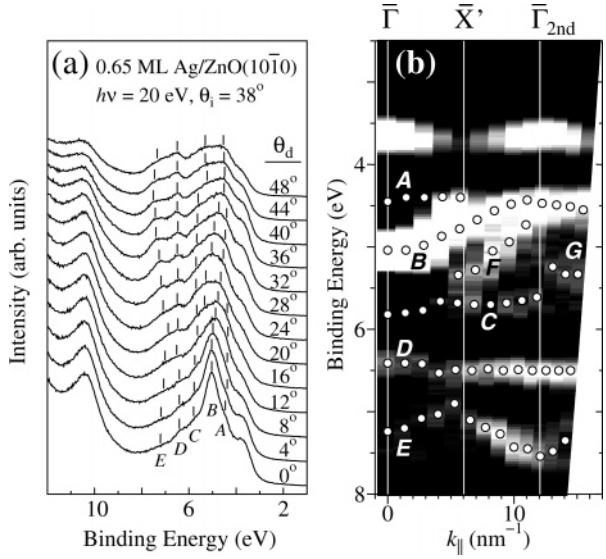

Figure 4. (a) Off-normal emission spectra of the 0.65-ML Ag-covered ZnO(10$\bar{1}$0) surface. The detection plane of the photoelectrons is set parallel to the [0001] direction. (b) The dispersion relation of the Ag 4d states (open circles) along the $\overline{\Gamma X'}$ axis of the SBZ of the substrate surface. The grayscale map is constructed from the second derivatives of the measured spectra in Figure 4a. Bright and dark parts correspond to high and low spectral weight, respectively. The O 2p band is observed at 3.5−4 eV.

measured kinetic energy, E_{kin}, using the equation

$$k_{\parallel} = \sqrt{2m_e E_{kin}/\hbar^2}\,\sin\theta_d$$

where m_e is the mass of the electron and $\hbar$ is the Planck constant divided by 2π. It is obvious that states *B* and *E* exhibit a strong dispersion along $\overline{\Gamma X'}$, whereas states *A*, *C*, and *D* disperse rather weakly. At large $k_{\parallel}$ ($\geq$5 nm^{-1}), other branches (*F* and *G*) are seen between 4.6 and 5.5 eV.

Figure 5 shows the Θ_{Ag}-dependent evolution of the Ag 4d bands along the $\overline{\Gamma X'}$ axis; (a) clean, (b) 0.12 ML, (c) 0.65 ML (reproduction of Figure 4b), and (d) 1.3 ML. On the clean surface, an intense O 2p dangling-bond band and weak bulk-related bands are seen at 3.5−4.5 eV and 4.5−8 eV, respectively. As the surface is being covered with Ag, the emission from the O 2p band becomes weaker, whereas the Ag 4d bands are developed. An important finding of these Θ_{Ag}-dependent measurements is that the basic structure of the Ag 4d bands is already formed at 0.12 ML and the dispersion relation of these bands undergoes only a minor change with increasing Θ_{Ag}. The formation of the dispersing bands at 0.12 ML means that the Ag adatoms should be condensed to give the lateral Ag−Ag interaction from the relatively low coverages. This is consistent with the conclusion drawn from the observed shift of the Ag 5sp DOS (Figure 2) that the Ag islands should be formed on the surface.

The dispersion of the Ag 4d bands means that $k_{\parallel}$ is a good quantum number in the Ag overlayer, that is, the Ag adatoms form some ordered structure. However, the LEED observations suggest the absence of the long-range ordered structure. Such an inconsistency should arise from the difference in the ordered domain size required for observing the LEED spots and for emerging the dispersing valence bands. In the LEED measurements using the primary energy of ~100 eV, which is a similar condition employed in the present study, an ordered domain with the size of at least ~10 nm is needed to give a diffraction pattern.[37] Contrastingly, a much smaller ordered domain is sufficient to give the dispersing valence bands. Tobin et al. have indicated from the layer-resolved ARPES study for Ag/Cu(001)[38] that the bulklike dispersion of the Ag 4d bands begins to be formed in the Ag overlayer with the thickness of 4−5 ML (1.2−1.5 nm). Moreover, the bulklike electronic structure is evolved in the metal clusters with ~100 atoms, whose diameter is around 1.5 nm.[34] Therefore, one scenario to consistently explain the LEED and ARPES results in the present study is that the Ag adatoms should form ordered domains with a size that is sufficiently large to give the dispersing Ag 4d bands (>1.5 nm) but is smaller than the detection limit by the LEED measurements (<10 nm). Considering that the Ag adatoms form islands as suggested by the shift of the Ag 5sp DOS (Figure 2), the Ag island should be composed of the Ag atoms with the lateral ordering, and each ordered domain could correspond to each Ag island.

Of the seven Ag 4d bands (*A*−*G*) seen in Figure 5, the behavior of band *G* is different from the other bands (*A*−*F*), that is, it grows with increasing Θ_{Ag}. Furthermore, as will be shown in the next section, band *G* is only an attenuated feature among the Ag 4d bands by annealing the Ag-covered surface. Although the origin of band *G* is not clear so far, it should be related to the state that is sensitive to the morphological change of the Ag overlayer, that is, it arises from the Ag adatoms that adsorb on top of the 2D islands.

Annealed Ag-Covered Surface. Figure 6 shows the comparison of the normal emission spectra obtained before and after annealing the 0.65-ML Ag-covered ZnO(10$\bar{1}$0) surface at 900 K for 3 min. The heat treatment results in a slight decrease in the emission intensity from the Ag 4d bands, whereas the intensity of the O 2p and Zn 3d peaks is somewhat recovered. As shown in the inset, the Ag 5sp emission in the gap region is also attenuated. These changes are due to either the decrease in the Ag coverage (if so, Θ_{Ag} is estimated 0.5 ML from the AES measurements) or the thickening of the Ag islands. In either case, sintering of the Ag islands should take place, as suggested by the shift of the onset energy of the Ag 5sp DOS from 0.17 to 0.12 eV, so that the size of each Ag island is increased either vertically and/or laterally.

The postannealed surface gives clear (1 × 1) LEED spots on the relatively low background intensity and integer-order streak lines along two orthogonal directions, which correspond to the [0001] and [$\bar{1}$2$\bar{1}$0] directions of the substrate surface. The observation of the clear LEED spots indicates that the ordered areas on the surface is enlarged. Moreover, the low background intensity results from the decrease in the number of the randomly distributed Ag adatoms. These random Ag adatoms should be absorbed partly by the Ag clusters and rearranged partly along the Zn−O dimer rows on the substrate surface at high temperatures. The rearranged Ag adatoms may be responsible for the streak lines in the LEED pattern.

Despite the change in the line shape of the normal emission spectrum by annealing at 900 K (Figure 6), the position of each Ag 4d peak is not affected much. Moreover, we have found similarities in the θ_d-dependent shift of the Ag 4d peaks in the off-normal emission spectra between the pre- and postannealed surfaces. In Figure 7a, the off-normal emission spectra of the postannealed surface along $\overline{\Gamma X}$ (the [$\bar{1}$2$\bar{1}$0] direction) and $\overline{\Gamma X'}$ (the [0001] direction) are presented. Figure 7b shows the dispersion relation of the Ag 4d states constructed from the spectra in Figure 7a.

Comparison of the 2D band structure along $\overline{\Gamma X'}$ between the preannealed (Figure 4b) and postannealed (the right half of Figure 7b) surfaces clarifies that the energetic position and the

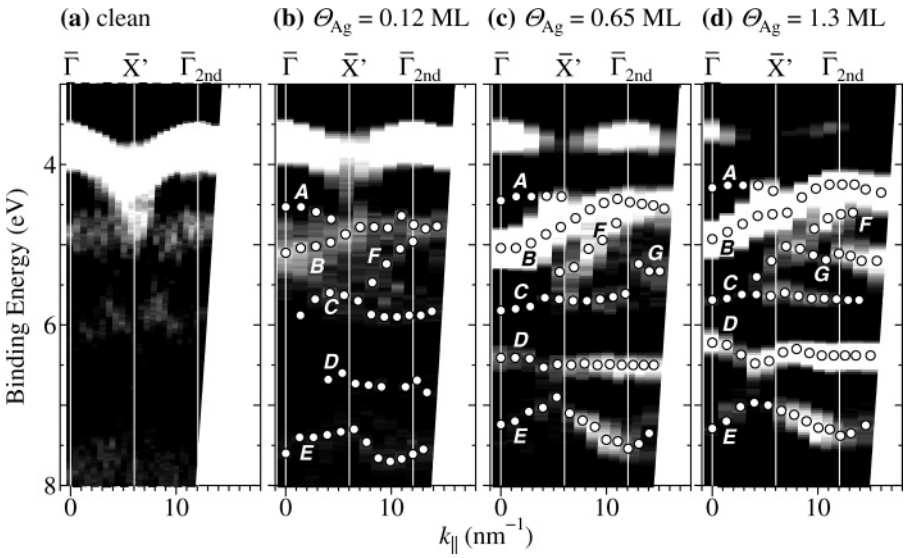

Figure 5. The 2D band structure of the ZnO(10$\bar{1}$0) surface along $\overline{\Gamma X'}$ as a function of the Ag coverage. Open circles indicate the position of the Ag 4d states.

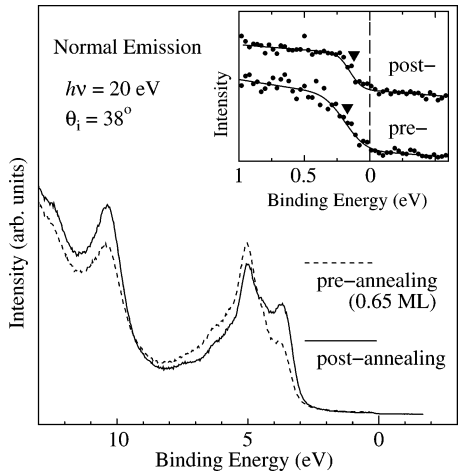

Figure 6. Normal emission spectra of 0.65-ML Ag-covered ZnO(10$\bar{1}$0) surfaces measured before (dashed curve) and after (solid curve) annealing at 900 K for 3 min. Suppression and evolution of the Ag 4d peaks and the substrate-related peaks, respectively, are observed by annealing the Ag-covered surface. The inset shows the enlarged spectra around the gap region. The triangles indicate the midpoint of the onset of the Ag 5sp DOS.

dispersion behavior of the Ag 4d bands are nearly identical on both surfaces except for band *G*, whose spectral weight is significantly attenuated on the postannealed surface. The fact that the band structure of Ag 4d states *A*−*F* is insensitive to annealing at 900 K suggests that the local atomic arrangement of Ag should be maintained despite the heat treatment.

The electronic structure of the Ag islands on the postannealed surface is characterized by intense band *B*. This band shows a positive dispersion around the $\bar{\Gamma}$ point and reaches the lowest binding energies at the $\bar{X}$ point ($k_{\parallel}$ = 9.67 nm^{-1}) along $\overline{\Gamma X}$ and at the $\bar{\Gamma}$ point in the second SBZ (Γ_{second}; 12.06 nm^{-1}) along $\overline{\Gamma X'}$. Similarly, the binding energy maxima of the deepest-lying bands (band *D* along $\overline{\Gamma X}$ and *E* along $\overline{\Gamma X'}$) coincide with $\bar{X}$ and $\bar{\Gamma}_{second}$. This, together with the LEED observation, implies that the ordered structure of the Ag domain is not completely incommensurate with the substrate surface but is strongly influenced by the surface structure of ZnO(10$\bar{1}$0).

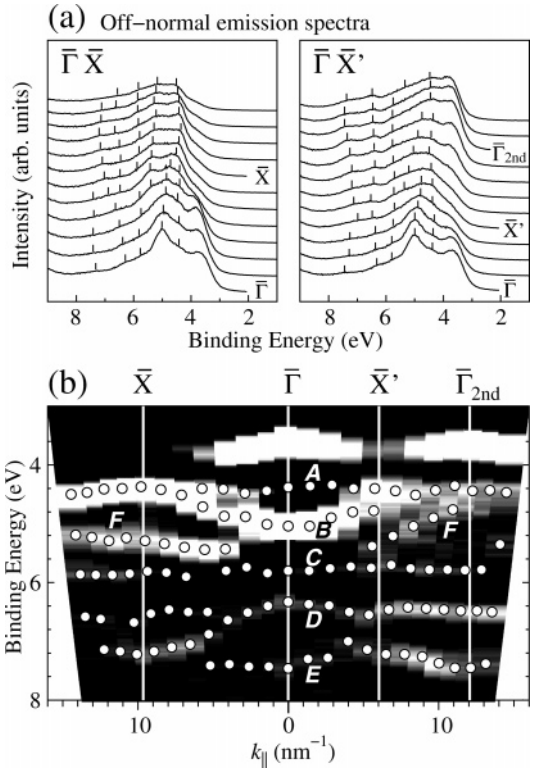

Figure 7. (a) Off-normal emission spectra of the postannealed Ag/ZnO(10$\bar{1}$0) surface along $\overline{\Gamma X}$ and $\overline{\Gamma X'}$. The spectra are measured at 20 eV with the emission angles from 0 to 44 ° at 4° intervals. (b) 2D band map of the postannealed Ag/ZnO(10$\bar{1}$0) surface along the $\overline{\Gamma X}$ and $\overline{\Gamma X'}$ axes of the SBZ. The Ag 4d bands are shown by open circles.

Discussion

Local Structure of Ag. The ARPES is a method that allows us to determine the energy and momentum of the emitted photoelectrons simultaneously and, hence, the valence band structure of the materials of interest. In the case of atomically disordered materials, for example, amorphous solid, the energy of the valence states does not depend on the crystal momentum. In contrast, the bulk and surface electronic structures of the atomically ordered materials are often characterized by the bands

with a dispersive feature. With these facts in mind, we first discuss the valence band structure of the Ag overlayer on the postannealed Ag/ZnO($10\bar{1}0$) surface.

As shown in Figure 7b, some of the Ag 4d states exhibit a clear dispersion along the $\overline{\Gamma X}$ and $\overline{\Gamma X'}$ axes of the SBZ. This means that Ag aggregates into islands with an ordered atomic structure. Assessing the Ag 4d band structure in more detail, one notices that the most intense band (*B*) and the deepest-lying band (*D* or *E*) have symmetric dispersion around the $\bar{X}$ point along $\overline{\Gamma X}$ and around the $\bar{\Gamma}_{\text{second}}$ point along $\overline{\Gamma X'}$. This is an indication that the ordered arrangement of Ag is influenced by the atomic structure of the ZnO($10\bar{1}0$) surface. The periodicity of the Ag bands seems to match that of the O 2p band at 3.5−4 eV along $\overline{\Gamma X}$, whereas the Ag bands along $\overline{\Gamma X'}$ could have the periodicity twice that of the O 2p band.

On the basis of this observation, we propose that the Ag adatoms on the annealed surface are arranged to form a 2D rectangular lattice, whose primitive vectors parallel to the $[\bar{1}2\bar{1}0]$ and [0001] directions of ZnO($10\bar{1}0$), with the nearest neighbor Ag−Ag distances which equal the lattice constant of ZnO($10\bar{1}0$) along the $[\bar{1}2\bar{1}0]$ direction ($a = 0.325$ nm[39]) and a half of the lattice constant along the [0001] direction ($c = 0.5206$ nm). Such a lattice matching between the substrate surface and the Ag overlayer is possible because the expected Ag−Ag distances in two directions (0.325 and 0.260 nm) are close to the neighboring distance between the Ag atoms in the bulk (0.289 nm[40]).

It should be pointed out that the proposed structure of the Ag adatoms do not affect the observed (1 × 1) LEED pattern on the annealed surface even if temperature-induced sintering leads to growth of the ordered Ag domains whose size exceeds ∼10 nm, which is needed to give the diffraction pattern as mentioned above. This is because the LEED spots from the ordered domain should overlap with the spots from the (1 × 1) substrate surface so that only the (1 × 1) LEED pattern is visible.

Next, we discuss the atomic structure of the vapor-deposited Ag overlayer at room temperature. Comparing the Ag 4d band structures of the pre- and postannealed Ag/ZnO($10\bar{1}0$) surfaces (Figure 4b and the right half of Figure 7b), it is clear that the dispersion of each Ag band is essentially the same for both surfaces except for the quenched band, *G*. Moreover, the Θ_{Ag}-dependent measurements of the Ag bands (Figure 5) reveal a similarity of the Ag bands throughout the submonolayer to near-monolayer coverage region. These results indicate that, in the [0001] direction, the ordered atomic arrangement similar to that formed on the annealed surface is already realized from the relatively low coverages.

Although the Ag 4d band structure is essentially the same irrespective of Θ_{Ag} along $\overline{\Gamma X'}$ (Figure 5), a Θ_{Ag} dependence is also noticeable. The binding-energy maximum and minimum in bands *B* and *E*, respectively, is located at the $\bar{\Gamma}_{\text{second}}$ point at $\Theta_{\text{Ag}} = 0.65$ and 1.3 ML. However, the minimum point in band *E* is observed at ~ 10 nm^{-1} at 0.12 ML. Similarly, the maximum point in band *B* seems to locate at smaller $k_{\parallel}$ at 0.12 ML. Such a $k_{\parallel}$ shift is considered to arise from a slight contraction of the lateral Ag−Ag distance along the [0001] direction. The nearest-neighbor distance can be roughly estimated to be ∼0.3 nm at 0.12 ML and is diminished to 0.26 nm at higher Θ_{Ag}. The enlargement of the dispersion width of some Ag bands (*B*, *D*, and *E*) supports the contraction of the Ag−Ag distance with increasing Θ_{Ag}.

Note that we have not measured the band structure of the vapor-deposited Ag overlayer along the $\overline{\Gamma X}$ axis, which corresponds to the direction parallel to the Zn−O dimer rows (the $[\bar{1}2\bar{1}0]$ direction). However, it is expected that deposited Ag atoms can diffuse readily along the dimer rows, as has been observed for Cu.[18] Therefore, the ordered Ag structure may be easier to form in the direction parallel to the Zn−O dimer rows than in the perpendicular direction.

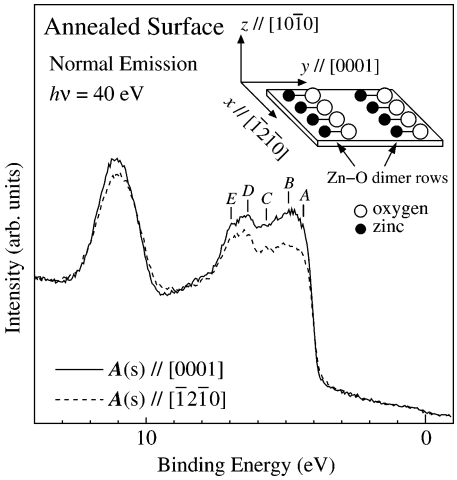

Figure 8. Normal emission spectra of the Ag/ZnO($10\bar{1}0$) surface annealed at 900 K. Both spectra were measured using *s*-polarized light, whose electric vector, ***A***, is parallel to the surface. Spectra acquired by the light with ***A*** || [0001] and ***A*** || $[\bar{1}2\bar{1}0]$ are, respectively, shown by solid and dashed curves. Both spectra are normalized to give an equal height at 13−14 eV.

Symmetry Analysis of the Ag 4d Bands. For the adsorption system of the Ag overlayer with rectangular symmetry on the ZnO($10\bar{1}0$) surface, it is possible to carry out the symmetry analysis of the Ag-derived states with respect to the mirror plane of the substrate surface. To better understand the electronic structure of Ag on ZnO($10\bar{1}0$), we have made the polarization-dependent ARPES measurements. Figure 8 shows the normal emission spectra of the postannealed Ag-covered surface measured by the *s*-polarized light, whose electric vector, ***A***, is parallel to the surface. The spectrum shown by a solid curve was obtained with [IMAGE]***A*** || [0001], whereas the dashed curve is the spectrum taken with ***A*** || $[\bar{1}2\bar{1}0]$. Both spectra are normalized to equal height at 13−14 eV in order to facilitate the comparison of the intensity variation of the Ag-derived peaks. The overall spectral line shape is different from the counterpart spectrum in Figure 6 because a different photon energy was used. However, we can still identify five Ag 4d peaks (*A*−*E*). Comparison of these two spectra clarifies that the emission intensity of all of the Ag states is smaller when measured by the light with ***A*** || $[\bar{1}2\bar{1}0]$ than with ***A*** || [0001]. However, a large attenuation is seen especially for peak *B* in comparison with other peaks.

According to the dipole selection rule for direct optical transition,[41] the initial states of the photoemission process can be distinguished by their symmetry with respect to the mirror plane of the crystal surface when using the polarized light. For the emission in the mirror plane, including the normal emission, the initial states must have the same symmetry with the electric vector of the light with respect to the mirror plane for the nonvanishing transition matrix element.

In the case of the Ag/ZnO($10\bar{1}0$) surface with C_s symmetry, where the mirror plane corresponds to the *yz*-plane (the coordination system is chosen as depicted in the inset of Figure 8), the initial states with even symmetry with respect to the mirror plane should be observed in the normal emission spectra when using the polarized light with ***A*** || [0001], and the states

with odd symmetry are accessible with $\boldsymbol{A} \parallel [\bar{1}2\bar{1}0]$. As shown in Figure 8, all of the Ag 4d peaks are attenuated in the spectrum taken by the light with $\boldsymbol{A} \parallel [\bar{1}2\bar{1}0]$. However, this should not mean that the Ag 4d states have odd symmetry. A weaker emission could be an artifact arising from the measurement geometry because the emission from the Zn 3d peak is also attenuated in the spectrum with $\boldsymbol{A} \parallel [\bar{1}2\bar{1}0]$. Although such an artifact is present, we can still guarantee that the intensity variation of peak *B* reflects the polarization dependence; namely, the enhancement of peak *B* by the light with $\boldsymbol{A} \parallel [0001]$ means that state *B* has even symmetry with respect to the mirror plane, that is, $d_{3z^2-r^2}$, $d_{x^2-y^2}$, or d_{yz}. State *B* disperses toward the lower binding energy side away from the $\bar{\Gamma}$ point along $\overline{\Gamma X'}$ and $\overline{\Gamma X}$ as shown in Figure 7b. On the basis of the tight-binding picture, only $d_{x^2-y^2}$ is the even state that has a positive dispersion along both high-symmetry axes in the Ag overlayer with rectangular symmetry. Therefore, the intense band, *B*, should be composed mainly of the $d_{x^2-y^2}$ orbitals.

Because the clear polarization dependence is not obtained for other bands, the symmetry argument is limited for band *B*. However, the dispersive feature of the band may allow us to further assign some of the Ag bands: band *D* could be associated with the d_{xy} or d_{yz} states because of the strong negative dispersion along the $\overline{\Gamma X}$ axis. Moreover, the slight positive dispersion of the deepest-lying band, *E*, in the vicinity of the $\bar{\Gamma}$ point hints the Ag 5s contribution, as suggested by the theoretical calculations that show the 5s character in the deepest-lying band in the hexagonal Ag monolayer.[43] The $d_{3z^2-r^2}$ state should form the dispersionless or a weakly dispersed band so that band *A* or *C* could be originated from this state. For more detailed and complete assignment of all Ag 4d bands, the spin−orbit and crystal-field splitting of the Ag 4d states, the influence of the ZnO($10\bar{1}0$) surface on the band structure of the Ag overlayer, the umklapp scattering of the emitted photoelectrons due to the different lattice constants between the Ag overlayer and the ($10\bar{1}0$) surface, and so forth, must be taken into account, and the help of the model calculation is desirable to understand the electronic structure of the Ag overlayer on ZnO($10\bar{1}0$) more completely.

The hexagonal Ag monolayers on the (111) and (100) surfaces of Cu and Ni exhibit the Ag 4d band structure characterized by a negatively dispersed band at 4−5 eV, which gives the most intense emission in the spectra taken with $h\nu = 21.2$ and 23 eV.[32,42] From the symmetry analysis, by assuming that the Ag monolayer has C_{6v} symmetry, Tobin et al. have proposed that the negatively dispersed band is composed of the E_1 states (d_{xz} and d_{yz}).[32] The different feature of the Ag 4d bands of the hexagonal Ag layers in comparison with the band structure found in the present system emphasizes a unique atomic structure of Ag on ZnO($10\bar{1}0$).

Growth Mode of Ag on ZnO($10\bar{1}0$). The Θ_{Ag}-dependent measurements of the Ag 4d band structure reveal that the dispersing Ag 4d bands are already formed at 0.12 ML (Figure 5b). Moreover, the onset position of the Ag 5sp DOS shifts toward E_F with increasing Θ_{Ag} (Figure 2). These results are indicative of the cluster formation by the Ag adatoms on ZnO($10\bar{1}0$).

A close examination of the Θ_{Ag}-dependent change and the annealing effect of the Ag 4d bands reveals that the origin of band *G* is different from that of bands *A*−*F*, that is, band *G* should be associated with the Ag adatoms that do not form the rectangular lattice. At high Θ_{Ag} on the Ag deposited surface, there should be some Ag adatoms on top of the Ag islands with the rectangular atomic arrangement, and these adatoms are eliminated easily via thermal desorption and/or diffusion upon annealing. The LEED observation supports the existence of such Ag adatoms because the blurred (1×1) spots on a bright background are observed on the vapor-deposited surface, whereas annealing results in sharper spots on the low background intensity. Thus, band *G* may be related to the Ag atoms adsorbed on top of the 2D Ag islands. This means that the Ag adatoms form the flat 2D islands at low Θ_{Ag} (at least up to 0.12 ML) and 3D growth starts at higher Θ_{Ag}; namely, growth of Ag on ZnO($10\bar{1}0$) proceeds via the 2D−3D transition of the Ag islands. From the behavior of band *G* as a function of Θ_{Ag}, a so-called "critical coverage" should be between 0.12 and 0.65 ML.

A recent STM study has revealed[18] that Cu forms islands on ZnO($10\bar{1}0$), and these islands are found to be exclusively 3D even at the very low coverages. Although Ag on ZnO($10\bar{1}0$) also clusterizes from the initial stages of adsorption, the clusters seem to have a monolayer thickness at low coverages and 3D growth starts from the moderate coverage. The growth mechanism of the metal overlayer is governed by several factors such as the thermodynamic equilibrium,[44,45] kinetics of the metal atoms on the surface,[15] and the atomic-level surface structures such as steps,[46,47] point defects,[48] and adsorbates.[18,49] The growth mode of Ag and Cu on the ZnO($10\bar{1}0$) surfaces must be influenced by all of these factors; however, the tendency can be explained on the basis of the thermodynamic stability of the metal-covered surfaces.

In thermodynamic equilibrium, when the sum of the surface free energy of deposited metals, γ_{metal}, and the interfacial free energy between the deposited metal and the substrate surface, γ_{int}, is larger than the surface free energy of the substrate, γ_{sub}, that is, $\gamma_{metal} + \gamma_{int} > \gamma_{sub}$, cluster growth should take place.[44,45] γ_{metal} of Cu is 2.1 Jm^{-2},[50] which is larger than that of the ZnO($10\bar{1}0$) surface ($\sim$1.2 Jm^{-2}).[51] γ_{metal} of Ag is approximately 1.2 Jm^{-2}.[50] Although γ_{int} is not available for both Ag/ZnO($10\bar{1}0$) and Cu/ZnO($10\bar{1}0$), a larger value is expected for the Cu adsorption system than for the Ag adsorption system because of the stronger interaction of Cu with the oxide surfaces than that of Ag as suggested from a series of the calorimetric measurements by Campbell and co-workers.[48] Although both systems fulfill the condition of cluster growth, the energy difference between $\gamma_{metal} + \gamma_{int}$ and γ_{sub} is smaller for Ag/ZnO($10\bar{1}0$) than that for Cu/ZnO($10\bar{1}0$). Therefore, deposited Ag tends to wet the ZnO($10\bar{1}0$) surface more preferentially than the Cu adatoms, and this is one of the reasons that the 2D island formation is possible in the case of the Ag/ZnO($10\bar{1}0$) system, whereas Cu forms the 3D islands from the very beginning.

Summary

The adsorption process and the 2D band structure of Ag on ZnO($10\bar{1}0$) have been investigated by ARPES utilizing synchrotron radiation. A characteristic dispersion of the Ag 4d bands, which does not resemble the band structure of the hexagonal Ag overlayers, is observed. Such a band structure is already developed at low coverages (0.12 ML), and the basic structure of the bands undergoes only a minor change up to 1.3 ML. These results indicate that Ag adsorption proceeds via the formation of the Ag islands with the ordered atomic arrangement. From the dispersion of the Ag 4d bands along the $\overline{\Gamma X'}$ and $\overline{\Gamma X}$ axes of the surface Brillouin zone of the substrate surface, the ordered structure is suggested to have rectangular symmetry with a good lattice matching with the ZnO($10\bar{1}0$) surface. It is also suggested that the Ag islands grow initially two-dimensionally at low coverages ($\leq$0.12 ML), and

3D growth sets in from a moderate coverage, which is well below the completion of the Ag monolayer. The critical coverage, where the 2D−3D transition occurs, should be between 0.12 and 0.65 ML. Such a growth mode is different from the previously revealed growth mode of Cu on ZnO($10\bar{1}0$), where exclusively 3D growth is observed. The different behavior of Cu and Ag on ZnO($10\bar{1}0$) is explained partly by the different wettability of the ($10\bar{1}0$) surface by Ag and Cu.

Acknowledgment. This work was performed under the approval of the Photon Factory Advisory Committee (proposal no. 2004G-007). We thank the staff of the Photon Factory for their excellent support. The work was financially supported by a Grants-in-Aid for Scientific Research (no. 14740374) from the Ministry of Education, Culture, Sports, Science and Technology of Japan.

References and Notes

(1) Haruta, M. *Catal. Today* **1997**, *36*, 153.
(2) Chusuei, C. C.; Lai, X.; Luo, K.; Goodman, D. W. *Top. Catal.* **2001**, *14*, 71.
(3) Chen, M. S.; Goodman, D. W. *Science* **2004**, *306*, 252.
(4) Bart, J. C. J.; Sneeden, R. P. A. *Catal. Today* **1987**, *2*, 1.
(5) Spencer, M. S. *Top. Catal.* **1999** *8*, 259.
(6) Nunan, J. G.; Bogdan, C. E.; Klier, K.; Smith, K. J.; Young, C. W.; Herman, R. G. *J. Catal.* **1989**, *116*, 195.
(7) Hoflund, G. B.; Epling, W. S.; Minahan, D. M. *Catal. Lett.* **1997**, *45*, 135.
(8) Breen, J. P.; Ross, J. R. H. *Catal. Today* **1999**, *51*, 521.
(9) Liu, S.; Takahashi, K.; Ayabe, M. *Catal. Today* **2003**, *87*, 247.
(10) Ammari, F.; Lamotte, J.; Touroude, R. *J. Catal.* **2004**, *221*, 32.
(11) Sakurai, H.; Haruta, M. *Catal. Today* **1996**, *29*, 361.
(12) Sugawa, S.; Sayama, K.; Okabe, K.; Arakawa, H. *Energy Conserv. Manage.* **1995**, *36*, 665.
(13) Mo, L.; Zheng, X.; Yeh, C.-T. *Chem. Commun.* **2004**, *12*, 1426.
(14) Ernst, K. H.; Ludviksson, A.; Zhang, R.; Yoshihara, J.; Campbell, C. T. *Phys. Rev. B* **1993**, *47*, 13782.
(15) Yoshihara, J.; Campbell, J. M.; Campbell, C. T. *Surf. Sci.* **1998**, *406*, 235.
(16) Yoshihara, J.; Parker, S. C.; Campbell, C. T. *Surf. Sci.* **1999**, *439*, 153.
(17) Koplitz, L. V.; Dulub, O.; Diebold, U. *J. Phys. Chem. B* **2003**, *107*, 10583.
(18) Dulub, O.; Boatner, L. A.; Diebold, U. *Surf. Sci.* **2002**, *504*, 271.
(19) Gaebler, W.; Jacobi, K.; Ranke, W. *Surf. Sci.* **1978**, *75*, 355.
(20) Roberts, S.; Gorte, R. *J. Chem. Phys.* **1990**, *93*, 5337.
(21) Petrie, W. T.; Vohs, J. M. *J. Chem. Phys.* **1994**, *101*, 8098.
(22) Radulovic, P. V.; Feigerle, C. S.; Overbury, S. H. *J. Phys. Chem. B* **2000**, *104*, 3028.
(23) Grant, A. W.; Ngo, L. T.; Stegelman, K.; Campbell, C. T. *J. Phys. Chem. B* **2003**, *107*, 1180.
(24) Chaturvedi, S.; Rodriguez, J.; Jirsak, T.; Hrbek, J. *Surf. Sci.* **1998**, *412/413*, 273.
(25) Ozawa, K.; Edamoto, K. *Surf. Sci.* **2003**, *524*, 78.
(26) Aiura, Y.; Bando, H.; Miyamoto, T.; Chiba, A.; Kitagawa, R.; Maruyama, S.; Nishihara, Y. *Rev. Sci. Instrum.* **2003**, *74*, 3177.
(27) Moormann, H.; Kohl, D.; Heiland, G. *Surf. Sci.* **1979**, *80*, 261.
(28) Jacobi, K.; Zwicker, G.; Gutmann, A. *Surf. Sci.* **1984**, *141*, 109.
(29) Mϕller, P. J.: Komolov, S. A.; Lazneva, E. F. *J. Phys.: Condens. Matter* **1999**, *11*, 9581.
(30) Ozawa, K.; Sawada, K. Shirotori, Y.; Edamoto, K.; Nakatake, M. *Phys. Rev. B* **2003**, *68*, 125417.
(31) Ozawa, K.; Sawada, K.; Shirotori, Y.; Edamoto, K. *J. Phys.: Condens. Matter* **2005**, *17*, 1271.
(32) Tobin, J. G.; Robey, S. W.; Shirley, D. A. *Phys. Rev. B* **1986**, *33*, 2270.
(33) Sprunger, P. T.; Lægsgaard, E.; Besenbacher, F. *Phys. Rev. B* **1996**, *54*, 8163.
(34) Wertheim, G. K.; DiCenzo, S. B.; Buchanan, D. N. E. *Phys. Rev. B* **1986**, *33*, 5384.
(35) Hövel, H.; Grimm, B.; Pollmann, M.; Reihl, B. *Phys. Rev. Lett.* **1998**, *81*, 4608.
(36) Howard, A.; Clark, D. N. S.; Mitchell, C. E. J.; Egdell, R. G.; Dhanak, V. R. *Surf. Sci.* **2002**, *518*, 210.
(37) Woodruff, D. P. *The Chemical Physics of Solid Surfaces and Heterogeneous Catalysis*; King, D. A., Woodruff, D. P., Eds.; Elsevier: Amsterdam, 1981; Vol. 1, p 81.
(38) Tobin, J. G.; Robey, S. W.; Klebanoff, L. E.; Shirley, D. A. *Phys. Rev. B* **1987**, *35*, 9056.
(39) Abrahams, S. C.; Bernstein, J. L. *Acta Crystallogr., Sect. B* **1969**, *25*, 1233.
(40) *CRC Handbook of Chemistry and Physics*, 76th ed.; Lide, D. R., Ed.; CRC Press: Boca Raton, FL, 1995.
(41) Hüfner, S. *Photoelectron Spectroscopy: Principles and Applications*; Springer-Verlag: New York, 1995; Springer Seriese in Solid-State Sciences Vol. 82, Chapter 6.
(42) Shapiro, A. P.; Hsieh, T. C.; Wachs, A. L.; Miller, T.; Chiang, T.-C. *Phys. Rev. B* **1988**, *38*, 7394.
(43) Nautiyal, T.; Youn, S. J.; Kim, K. S. *Phys. Rev. B* **2003**, *68*, 033407.
(44) Campbell, C. T. *Surf. Sci. Rep.* **1997**, *27*, 1.
(45) Diebold, U. *Surf. Sci. Rep.* **2003**, *48*, 53.
(46) Chen, D. A.; Bartelt, M. C.; Hwang, R. Q.; McCarty, K. F. *Surf. Sci.* **2000**, *450*, 78.
(47) Chen, D. A.; Bartelt, M. C.; Seutter, S. M.; McCarty, K. F. *Surf. Sci.* **2000**, *464*, L708.
(48) Campbell, C. T.; Starr, D. E. *J. Am. Chem. Soc.* **2002**, *124*, 9212.
(49) Grant, A. W.; Ranney, J. T.; Campbell, C. T.; Evans, T.; Thornton, G. *Catal. Lett.* **2000**, *65*, 159.
(50) Vitos, L.; Ruban, A. V.; Skriver, H. L.; Kollár, J. *Surf. Sci.* **1998**, *411*, 186.
(51) Meyer, B.; Marx, D. *Phys. Rev. B* **2003**, *67*, 035403.